# Enhancing turbulent fluctuation measurement with tailored wind lidar profilers

Maxime Thiébaut [1], Frédéric Delbos [2], Cristina Benzo [2], Loïc Mahe [2], and Florent Guinot [1]

[1]France Énergies Marines, Technopôle Brest-Iroise, 525 Avenue Alexis de Rochon, 29280 Plouzané, France
[2]Vaisala France SAS, 6A, rue René Razel, Tech Park, CS 70001, 91400 Saclay Cedex, France

**Correspondence:** Maxime Thiébaut (maxime.thiebaut@france-energies-marines.org)

**Abstract.** This study separately investigates the impact of an enhanced sampling rate and reduced probe length on turbulent measurements using the Vaisala WindCube v2.1 lidar profiler, in comparison to the commercially configured WindCube v2.1. In the first experiment, a tailored lidar sampled four times faster than the standard setup. In the second experiment, a tailored lidar employed a 15 m probe length, compared to the commercial configuration's 23 m. The study offers a detailed analysis of how these changes affect various aspects of wind measurement, including mean wind speed, standard deviation, velocity spectra, noise level, integral length scale, and dissipation rate. Increasing the sampling rate improves turbulence measurement without affecting mean wind speed measurement. However, a slight reduction in data availability was observed compared to the commercial configuration. Reducing the probe length results in higher standard deviation values compared to the commercial configuration, but this comes at the expense of increased noise levels, making it unclear whether the higher standard deviations are due to the energy of smaller eddies or noise. Additionally, the reduced probe length configuration exhibited a high bias in mean wind speed measurement and had a limited impact on other turbulence metrics. These findings suggest that the best improvement for turbulence measurement with the WindCube lidar profiler is achieved through an increased sampling rate.

## 1 Introduction

Accurate turbulence data enables better understanding and control of wind flow patterns, optimizing the design, operation, and maintenance of wind energy systems. Furthermore, turbulence measurement plays a pivotal role in addressing key challenges within the wind energy sector. It aids in enhancing the efficiency and safety of wind turbine operations, minimizing wear and tear on vital components, and extending the lifespan of these costly assets. Additionally, improved turbulence measurement can facilitate more precise wind resource assessments, aiding in site selection and the overall planning of wind energy projects.

In the wind energy sector, the utilization of wind lidar profiler technology has gained significant traction in recent years, supplanting the traditional meteorological mast equipped with in-situ sensors like cup or sonic anemometers as the standard means of measuring key mean wind properties, such as speed and direction. Lidar profilers present compelling advantages, including the potential for cost reduction compared to meteorological masts and the capacity to measure at similar or even greater heights above the ground.

Measurement methods used by lidar profiler are fundamentally different than those used by cup or sonic anemometers.
25 Anemometers provide an estimate of the wind speed across a volume of few cubic centimeters whereas lidars provide an average across a probe volume of up to several dozen cubic meters. Lidars can be categorized according to their emission waveform, i.e., pulsed or continuous, and measuring technique, i.e., Doppler beam swinging (DBS) (Strauch et al., 1984) or velocity-azimuth display (VAD) (Browning and Wexler, 1968).

However, lidar profilers have yet to garner widespread acceptance for turbulence measurement, which remains a focal point
30 of ongoing research. In contrast to turbulence data derived from reference instruments such as sonic anemometers, turbulence data derived from lidar profiler measurements suffer from systematic errors induced by, (i), the inter-beam effect, also known as the cross-contamination effect, (ii), the intra-beam effect, i.e, the averaging effect of the probe volume, (iii), low sampling rate and, (iv), noise. The inter-beam effect can lead to either underestimation or overestimation of turbulence metrics (Kelberlau and Mann, 2020). This discrepancy arises from the modulation of energy associated with eddies characterized by
35 specific wavenumbers. The intra-beam effect is a consequence of the probe length, effectively acting as a low-pass filter. This phenomenon stems from the filtering out of eddies that fall beneath the size threshold set by the probe length, generating underestimation of turbulence metrics.

Lidar profilers require several seconds to complete a full scanning circle, resulting in a low sampling rate that causes discrepancies between turbulence measurements taken by anemometers and those by lidar profilers (e.g., Peña et al., 2009). Turbulent
40 motion scales can vary from milliseconds to hours and from centimeters to kilometers (e.g., Stull, 2000), but lidars are limited to measuring turbulent motions with timescales of seconds and spatial scales of tens of meters. However, wind turbine components are influenced by various scales of turbulent structures, making it crucial to detect a broad range of smaller turbulence scales.

The concept of measuring turbulence using remote sensing instruments has gradually evolved since the early works in radar
45 meteorology by Lhermitte (1962) and Browning and Wexler (1968). Lhermitte (1969) was the first to propose a method for inferring turbulence by analyzing the variance of radial velocity measurements through VAD scanning. Following this, Wilson (1970) conducted pioneering experiments using a pulsed Doppler radar to detect turbulence within the convective boundary layer (0.1-1.3 km). However, these early measurements were limited to turbulence scales larger than the pulse volume and smaller than the scanning circle, and no validation against reference instruments was performed, questioning their reliability.
50 Kropfli (1986) expanded Wilson's approach to capture turbulence scales larger than the scanning circle by integrating data from multiple scans. Although initially developed for Doppler radar, these methods were later adapted for Doppler lidar. Eberhard et al. (1989) were the first to apply Wilson's and Kropfli's methods using lidar, and Gal-Chen et al. (1992) further refined the technique with a different scanning configuration. Despite these advancements, the significant probe length (around 100 m) limited studies to the convective boundary layer due to considerable probe volume averaging, especially near the
55 ground. To address this limitation, research shifted towards understanding and mitigating probe volume averaging effects (e.g., Smalikho et al., 2005; Mann et al., 2010; Branlard et al., 2013). Nowadays, modern lidar systems have reduced probe lengths to about 30 m, but averaging effects still pose challenges for turbulence measurements in the surface layer where wind turbines operate (e.g., Mann et al., 2009; Sjöholm et al., 2009; Sathe et al., 2011; Sathe and Mann, 2012).

Considering the pivotal role of turbulence measurement in wind energy applications, the past decade has seen significant advancements in the development and customization of wind lidar technology. Notably, a study by Sathe et al. (2015) proposed a novel six-beam method for measuring turbulence using a Vaisala pulsed lidar Windcube 200. This method involves capturing line-of-sight (LOS) velocity fluctuations at five equally spaced azimuth angles along the base of a scanning cone and a sixth measurement at the center of the scanning circle using a vertical beam at the same height. When compared to the traditional VAD method, which often results in significant averaging effects on measured turbulence, the six-beam approach offers improved accuracy. Specifically, the six-beam method was found to measure 85-101% of the reference turbulence indicated by a cup anemometer, whereas the VAD method measured only 66-87% of the reference turbulence, depending on atmospheric stability and the wind field component.

The present paper aligns with this trajectory, as it delves into the specific advancements pertaining to the Vaisala WindCube v2.1 lidar profiler. Two key modifications are explored: first, an augmentation of the sampling rate, and second, a reduction in the probe length. These customizations are individually evaluated for their impact on the measurement of mean wind statistics such as the mea, wind speed and turbulent metrics such as the standard deviation of wind velocity, the velocity spectra, the vertical integral length scale and the dissipation rate. The impact of noise on both modifications is also evaluated. Notably, this study does not address the combined effects of both modifications.

## 2 Data and methods

### 2.1 Modifications to the WindCube v2.1 lidar system

#### 2.1.1 Increased sampling rate

The WindCube v2.1 lidar profiler employs a DBS technique for measuring wind speed. This technique involves the use of an optical switch to alternately direct the lidar beam in the four cardinal directions (north, east, south, and west), each at an inclination angle of 28° from the vertical. Subsequently, the beam is directed vertically upwards, providing measurements from a total of five distinct positions (Fig. 1a). In its standard commercial configuration, the WindCube lidar collects data at each location in 1 second and steers the beam to the next location. This process completes a full DBS scan in 4 seconds, resulting in a sampling rate of 0.25 Hz for LOS velocity and 1 Hz for wind speed.

These frequencies are well-suited to capture turbulent structures with dimensions of 100 m and beyond. However, it's worth noting that wind turbine components are affected by turbulent structures across various scales. As a result, it becomes essential to increase the lidar profiler's sampling rate to encompass a more comprehensive velocity spectrum, enabling the capture of turbulence structures at smaller scales that also impact wind turbine components.

In response to the demand for increased sampling rate, we have engineered a tailored iteration of the WindCube v2.1. This enhanced version operates four times faster, providing a LOS velocity and wind speed sampling rate of 1 Hz and 4 Hz respectively. This improvement was achieved by reducing the accumulation time for data collection from each beam by 70%, in
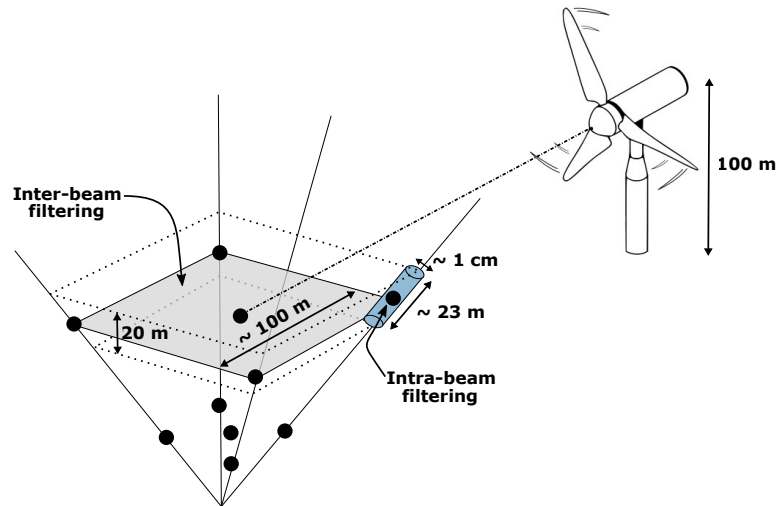
**Figure 1.** Schematic illustration of inter and intra-beam filtering effects in WindCube v2.1 lidar profiler measurement process. The blue cylinder represents a probe with dimensions matching the commercial lidar configuration.

conjunction with a corresponding 70% reduction in the number of transmitted pulses. Please note that specific details regarding the accumulation time and pulse count cannot be disclosed publicly.

The dataset used to assess the impact of the increased sampling rate on the measurement of turbulent fluctuations encompasses a 47-day period, split into 2256 30-min subsets, spanning two time intervals: from November 12 to November 25, 2021, and from December 7, 2021, to January 10, 2022. During this campaign, lidar measurements were recorded at ten different heights ranging from 40 to 200 m above ground level. This measurement campaign was conducted as part of the lidar test verification performance at the Janneby site, Germany, overseen by DNV-GL. The commercial lidar configuration and a prototype version with an enhanced sampling rate, positioned approximately 14 m apart, were tested against a meteorological mast equipped with cup and sonic anemometers. Both configurations successfully passed the test. Please note that this paper does not discuss the measurements obtained from the anemometers.

### 2.1.2 Reduced probe length

The intra-beam filtering effect (Fig. 1) is a result of the probe length, which effectively acts as a low-pass filter by selectively attenuating eddies smaller than the probe length. This phenomenon occurs because it filters out eddies smaller than the size threshold defined by the probe length, denoted as $\Delta z$ (with units of length). The pulse length (with units of time), $T$, determines the probe length, and in the case of the WindCube v2.1 lidar, multiple pulses are sent into the atmosphere. Each pulse occupies a volume in the atmosphere at time $t$, defined by $\Delta z = cT/2$, where $c$ represents the speed of light (Fig. 2).

In its standard commercial configuration, the WindCube v2.1 measures LOS velocity within a probe of approximately 23 m (Fig. 1). This corresponds to a certain Transistor-Transistor Logic (TTL) pulse duration, the specific value of which cannot be
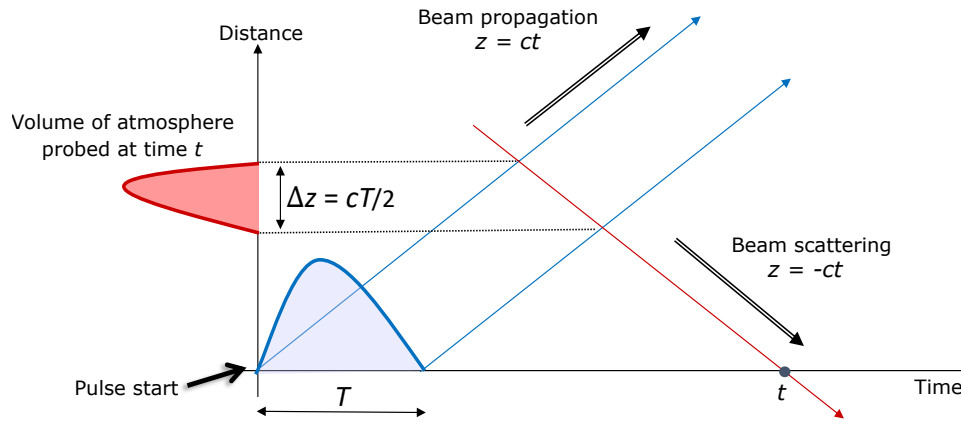
**Figure 2.** Length, $\Delta z$, of the probe is expressed as a function of pulse length, $T$, and speed of light, $c$.

publicly disclosed. The tailored version of the WindCube v2.1 lidar features a 50% reduction in pulse duration, leading to a reduction in the probe length from 23 m to 15 m.

The dataset used to evaluate the impact of the reduced probe length on the measurement of turbulent fluctuations spans 4 days, from May 31, 15:00 (UTC 0) to June 04, 15:00 (UTC 0), 2023, divided into 240 30-minute subsets. Throughout this observational campaign, both the commercial and tailored lidar systems, separated by less than 1 m, collected data at ten distinct heights, ranging from 40 m to 200 m above the lidar instruments. These measurements were conducted on the experimental terrace, located atop the Vaisala office in Saclay, France. The commercial lidar was a "Golden Lidar", meaning it is a reference lidar that has been verified against an IEC-compliant met mast by a third party.

## 2.2 Evaluation metrics

Our investigation is centered around evaluating the impact of two key enhancements on the WindCube v2.1 lidar profiler: (1) increasing the sampling rate and (2) reducing the probe length. We conduct two distinct measurement campaigns, each focusing on a single enhancement at a time. To establish a baseline, we gather wind speed and turbulence measurements using the commercially configured WindCube v2.1 system. These initial measurements serve as a reference point against which we can effectively assess the effects of the enhancements in both increased sampling rate and reduced probe length.

Our study commences by analyzing the effects of the lidar enhancements on the 10-minute average wind speed, $U$, and data availability. Subsequently, we shift our focus to turbulence analysis, derived from 30-minute subsets of data.

### 2.2.1 Standard deviation

In this study, we focus on analyzing velocity fluctuations as the primary turbulence metric, quantified through the calculation of standard deviation. Assessing the standard deviation of wind velocity fluctuations is essential in wind energy applications.

It offers insights into turbulence intensity, aids in estimating dynamic loads on turbine components, enhances power prediction models, informs turbine control strategies, and supports site assessment for optimal wind farm development and operation.

The standard deviation of the mean velocity along and across the wind propagation, denoted as $\sigma_u$ and $\sigma_v$ respectively were quantified in this study. To achieve this, we first rotate the velocity measured along the lidar's $x$-axis, denoted as $V_x$ and aligned with true North, such that the mean velocity along the $y$-axis, noted as $V_y$, becomes 0. The wind velocity along the $x$-axis is then aligned with the 30-minute mean wind direction. The expressions for $V_x$ and $V_y$ are given by Eq. 1 and 2:

$$V_x = \frac{b_3 - b_1}{2 \sin\phi} \tag{1}$$

$$V_y = \frac{b_4 - b_2}{2 \sin\phi} \tag{2}$$

Here, $\phi = 28°$ represents the zenith angle, and $b_i$ denotes the LOS velocity measured by each beam $i$, with positive velocity directed towards the instrument.

Furthermore, we investigate the standard deviation, $\sigma_5$, of the mean vertical velocity, through direct measurement of the vertical component of the wind speed provided by beam 5.

### 2.2.2   Integral length scale

Understanding the integral length scale helps in quantifying the spatial extent of turbulence within a wind field. This information is essential for assessing the potential impact of turbulence on the performance and structural integrity of wind turbines. Moreover, integral length scale data is often used as input for turbulence models employed in wind energy simulations. These models help predict wind turbine loads, fatigue, and power output by accounting for the effects of turbulence on the flow field.

The 5-beam configuration of the WindCube v2.1 lidar enables the computation of the vertical integral length scale, denoted as $L_w$, propagating along the horizontal flow trajectory, through direct measurements of the vertical velocity by beam 5. However, quantifying the along and across-wind integral length scales, i.e., $L_u$ and $L_v$ respectively, requires wind alignment with one pair of opposite beams.

The integral length scale, $L_j$, associated with the direction $j$ can be estimated by calculating the integral timescale, $\Lambda_j$. The latter serves as a measure of the duration during which the largest eddies maintain correlation. For each 30-minute interval, $\Lambda_j$ is computed from a temporal autocorrelation function, $R_{jj}(\tau)$, integrated over time from $\tau = 0$ to the first instance of $R_{jj} = 0$ (e.g., Tritton, 2012). For the example of the vertical wind component, the integral timescale, $\Lambda_w$, is given by:

$$\Lambda_w = \int_{\tau=0}^{\tau[R_{ww}(\tau)=0]} R_{ww}(\tau)\mathrm{d}\tau \tag{3}$$

with the temporal autocorrelation function defined as:

$$R_{ww}(\tau) = \frac{R\left[b_5'(t), b_5'(t+\tau)\right]}{\sigma_{b_5}^2} \tag{4}$$

where the prime denotes a fluctuation from the mean. The integral length scale, $L_w$, is estimated by invoking Taylor's frozen turbulence hypothesis:

$$L_w = \Lambda_w U \tag{5}$$

### 2.2.3 Velocity spectra

Power spectral density of the velocity, i.e., the velocity spectra, provide valuable information about the distribution of turbulent kinetic energy across different scales of motion within the wind flow. This understanding helps in characterizing turbulence and its effects on wind turbine performance and structural loads.

Velocity spectra were computed using Welch's method (Welch, 1967). This method computes an estimate of the spectrum by dividing the data into overlapping segments, computing a modified periodogram for each segment and averaging the periodograms. The Hann window with 50% overlap was applied to each segment to reduce spectral leakage and improve frequency resolution. The 50% overlap is a reasonable trade off between accurately estimating the signal power, while not over counting any of the data.

Velocity spectra $S_5(f)$, of the LOS velocities measured by beam 5 were computed for each 30-min subsets. The spectra were fitted by a parametric expression (Teunissen, 1980; Olesen et al., 1984; Tieleman, 1995) in the frequency domain $f$, to which we add a component $N_5$ associated with the power spectral density of noise of the LOS velocity measured by beam 5 (see section 2.2.4):

$$S_5(f) = \frac{m}{(1+nf)^\beta} + N_5 \tag{6}$$

The coefficient $m$ primarily controls the vertical scaling or amplitude of the spectum whereas $n$ influences the rate at which the function decays as $f$ increases. The exponent $\beta$ determined the shape of the spectrum.

### 2.2.4 Noise

Doppler noise is a critical factor in the spectral analysis of velocity time series. This type of noise arises from random fluctuations in the frequency of a signal due to the relative motion between the source and the observer. In the spectrum of a velocity time series, Doppler noise typically manifests as a flattening of the spectrum at higher frequencies, indicating a white noise characteristic that contributes equally across these frequencies (e.g., Thomson et al., 2012; Durgesh et al., 2014; Guerra and Thomson, 2017; McMillan and Hay, 2017; Thiébaut et al., 2020a). At lower frequencies, the spectrum is usually dominated by the actual signal, which may show a characteristic decay or specific features related to the physical process being measured, such as turbulence. As frequency increases, the influence of Doppler noise becomes more prominent, leading to a flattened spectral region where the noise dominates.

In Eq. 6, $N_5$ represents the constant Doppler noise level, which contributes to the spectral flattening observed at higher frequencies. This understanding is particularly important in the context of turbulence measurement, where accurately distin-
185 guishing between the actual turbulent signal and noise is crucial for comprehending the dynamics and energy distribution within a turbulent flow. Doppler noise can obscure the true signal at higher frequencies, complicating the analysis and potentially leading to erroneous conclusions if not properly accounted for. Failure to account for this noise can result in an overestimation of turbulence metrics such as the dissipation rate (Bodini et al., 2018). The variance of the noise depends on the technical characteristics of the device measuring the velocity, such as Nyquist velocity, the signal spectral width, the number
190 of pulses and points per range gate, and the signal-to-noise ratio. Theoretical expressions for the variance of this noise can be derived and subsequently removed from the computed turbulence metrics to improve accuracy (O'Connor et al., 2010; Bodini et al., 2018, 2019; Wildmann et al., 2019). However, the technical specifications of lidar profilers are no longer openly shared with users, making it impossible to evaluate this noise theoretically. Therefore, it is necessary to determine this noise using a spectral approach, such as the one presented in this paper.

195 **2.2.5 Dissipation rate**

The dissipation rate, $\varepsilon$, quantifies the rate at which turbulent kinetic energy is converted into thermal energy within the atmosphere. Measuring dissipation is crucial for validating atmospheric circulation models, which are essential for accurate wind resource assessments. By providing detailed information about turbulence within the wind flow, the dissipation rate helps improve the precision of these models. This leads to better predictions of wind patterns and energy potential, ultimately enhancing
200 the planning and optimization of wind farms.

The characterization requires the identification of the inertial subrange of turbulence, i.e., the range of scales within a turbulent flow where energy cascades from larger to smaller eddies without significant loss to viscosity. In the context of three-dimensional turbulence, the spectrum, $S(k)$, in the inertial subrange is often described by Kolmogorov's -5/3 law and is proportional to $k^{-5/3}$, where $k$ is the wavenumber, inversely proportional to the size of the eddies. This scaling indicates that
205 the energy density decreases with increasing wavenumber (or decreasing eddy size) in a predictable manner. The spectrum, $S_5(k)$, of the vertical velocity measured directly by beam 5 can be related to the dissipation rate as follows:

$$S_5(k) = C_w \varepsilon^{2/3} k^{-5/3} + \hat{N}_5 \tag{7}$$

with $C_w = 0.69$ is the universal Kolmogorov constant (Sreenivasan, 1995; Pope, 2000) and $\hat{N}_5$ the power spectral density of noise in the wavenumber domain.

210 The transition wavelength $\lambda_w$ between the inertial subrange and the outer scales can be expressed as a function of the integral scale $L_w$ (Eq. 5) and the parameter $\mu$:

$$\lambda_w = \left[ \frac{5}{3} \sqrt{\mu^2 + \frac{6}{5}\mu + 1} - \left( \frac{5}{3}\mu + 1 \right) \right]^{1/2\mu} \frac{2\pi}{C_w} L_w \tag{8}$$

Where $\mu = 1.5$ as proposed in several studies (e.g., Lothon et al., 2009; Tonttila et al., 2015; Bodini et al., 2018). These values have been found to provide a good match to most of the observed spectra presented in these studies. Following the

approach in Tonttila et al. (2015), one can estimate the timescale, $t_w$, corresponding to this transition wavelength by dividing $\lambda_w$ by the collocated wind speed, $U$. The transition frequency, $f_a$, between the area of the outer scales of turbulence and the inertial subrange, is then given by $f_a = 1/t_w$. Finally, the transition frequency, $f_b$, between the inertial subrange and the noise-dominated range is set to $f_b \approx 0.8 f_N$, where $f_N$ is the Nyquist frequency. This value of $f_b$ aligns with findings from other studies that identify the noise-contaminated frequency domain in devices using the Doppler effect to measure flow velocity (e.g., Frehlich, 2001; Bodini et al., 2018; Thiébaut et al., 2020b).

From Eq. 7, one can deduce the dissipation rate by invoking Taylor's 'frozen field hypothesis,' which assumes that the turbulence is in a steady state as it advects past the instrument, meaning it is neither developing nor decaying. Under this assumption, one can transform spatial observations into temporal observation, using the relation $f = Uk/2\pi$. The dissipation rate, $\varepsilon$, is thus given by (McMillan and Hay, 2017; Thiébaut et al., 2022):

$$\varepsilon = \left( C_w^{-1} [S_5(f)|_{f_a}^{f_b} - N_5] \, f^{5/3}\Big|_{f_a}^{f_b} \left( \frac{2\pi}{U} \right)^{5/3} \right)^{3/2} \tag{9}$$

This equation applies under the assumption that the inertial subrange follows the classic -5/3 slope. Computing the dissipation rate from the vertical velocity measured directly by beam 5 of the WindCube v2.1 lidar involves a two-step process. The first step is to determine the power spectral density of $S_5(f)$ between frequencies $f_a$ and $f_b$. For this step, it is recommended to fit the measured velocity spectrum using Eq. 6 with $\beta = 5/3$. However, it will be demonstrated in this paper that setting $\beta$ to this specific value has shown difficulties in accurately representing noise (see Section 3.3). Therefore, it is advisable to set $N_5 = 0$ for the computation of the mean power spectral density. In the second step, the power spectral density of noise, $N_5$, is computed by performing a second fitting where $\beta$ is allowed to vary freely. This $N_5$ is then subtracted from the mean spectral density of $S_5(f)$ computed between $f_a$ and $f_b$ in the first step. This approach ensures that $N_5$ accurately represents noise contributions while allowing flexibility in $\beta$ during the fitting process.

## 3 Results

### 3.1 Data availability and mean wind speed

The first step when proposing enhancements to lidar technology is to evaluate their impact on data availability of the wind vector. This evaluation was conducted at each measurement height for both enhancements proposed for the WindCube v2.1 lidar profiler. The reduction of probe length did not impact data availability, which remained close to 100% at each measurement altitude for both the commercial and prototype configurations. However, increasing the sampling rate slightly affected data availability. The commercial configuration showed data availability ranging from 99.7% at the first measurement height to 93.2% at the last measurement height, whereas the prototype configuration showed data availability consistently lower by less than 0.5%.
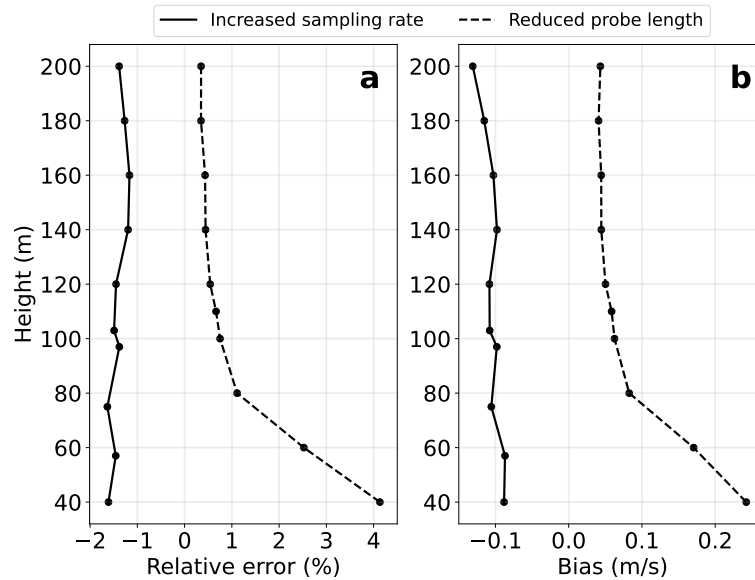
**Figure 3.** Relative error (a) and bias (b) in mean wind speed measurements of the prototype lidars involving an increase in the sampling rate (solid line) and a reduction in the probe length (dashed line), compared to the mean wind speed measured by a commercial lidar, which serves as the reference measurement.

Next, the effectiveness of the prototype configurations was evaluated by testing their ability to measure wind speed aver-

245 aged over a 10-minute interval. To pass the "Best Practice" standard, a lidar profiler has to demonstrate mean wind speed measurements that differ by no more than $\pm 1\%$ from the mean wind speed measured by a reference measurement, such as a cup anemometer (International Electronical Commission, 2017). An absolute difference between $1\%$ and $1.5\%$ is considered acceptable under the "Minimum Practice" standard. If the absolute difference exceeds $1.5\%$, the lidar cannot be certified for mean wind speed measurement.

250 Here, the mean wind speed measured by the first prototype lidar involving an increase of sampling rate and the second prototype lidar involving a reduction of the probe length was compared to mean wind speed measured by a commercial lidar serving as reference measurement. The mean relative error and the bias were calculated at each measurement height. Fig. 3 illustrates that an increase in the sampling rate leads to a systematic underestimation of the mean wind speed. This underestimation is nearly constant across different altitudes, averaging $1.3\%$, which corresponds to a bias of approximately 0.1

255 m/s. Conversely, reducing the probe length results in a systematic overestimation of the mean wind speed. This overestimation manifests in two distinct patterns: above 100 m, where the prototype lidar overestimates the mean wind speed by an average of $0.5\%$, and below 100 m, where a significant overestimation occurs, peaking at over $4\%$ resulting in a bias of 0.2 m/s, observed at the first measurement level, 40 m above the ground.

The bias in mean wind speed measurements associated with a reduced probe length is illustrated in Fig. 4. The goal is to

260 identify potential parameters that could influence this high bias at lower altitudes. Fig. 4a shows that wind speed does not
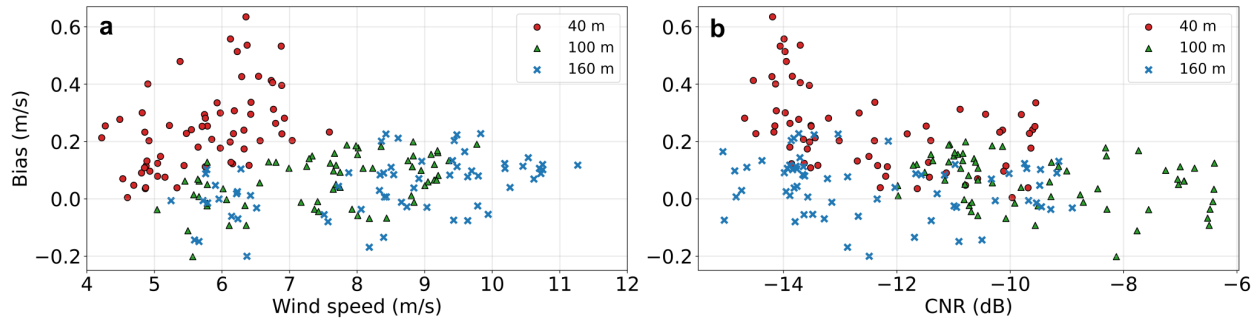
**Figure 4.** Bias variation in mean wind speed measurement: comparison by mean wind speed (a) and CNR (b).

influence the bias. Although the lowest wind speed at 40 m could explain the high bias (i.e., more than 0.4 m/s), this does not hold, as similar mean wind speeds were measured at higher altitudes with less than half the bias. The carrier-to-noise ratio (CNR), an output data of the lidar, was also investigated as a potential source of bias (Fig. 4b). Despite the significantly higher bias at 40 m compared to that at 160 m, similar CNR values were recorded at both 40 m and 160 m above the ground.

265 **3.2 Standard deviation**

Estimates of the standard deviation measured by the prototype lidars compared to those computed from the commercial lidars are presented in Fig. 5. The regression analysis showed linear relationships with slopes ranging from 0.9 to 1.022 and positive intercepts, all with $R^2$ values consistently above 0.9. Both the mean and median of the standard deviations were systematically higher for the increased sampling rate and reduced probe length configurations. Specifically, the mean standard deviation

270 of the along-wind, cross-wind, and vertical velocities for the increased sampling rate configuration was between 3.5% and 6.3% higher than those from the commercial configuration (Fig. 5a). For the reduced probe length configuration, the mean standard deviation was between 0.3% (for along-wind velocity) and 3.4% higher (Fig. 5b). Additionally, the interquartiles of the standard deviation provided by the prototype configurations were consistently higher than those from the commercial configuration, indicating greater variability and sensitivity in the measurements. Furthermore, the vertical evolution of the mean

275 standard deviation showed that both modifications resulted in higher standard deviations at each altitude, with the discrepancy from the commercial configuration increasing with height (Fig. 7). Notably, the gaps were more than twice as large at the highest measurement altitude compared to the lowest.

**3.3 Velocity spectra**

The analysis of LOS velocities obtained from beam 5 involved computational fitting using a parametric expression (Eq. 6).

280 Various weighting schemes were systematically explored to enhance fitting accuracy and minimize errors relative to the measured spectra. Assessing the fitting accuracy included comparing the variance, denoted as $\sigma_5^2$, obtained from the integrated fitted spectra with the measured spectra, and calculating their absolute relative differences. Fig. 8 illustrates an example of the
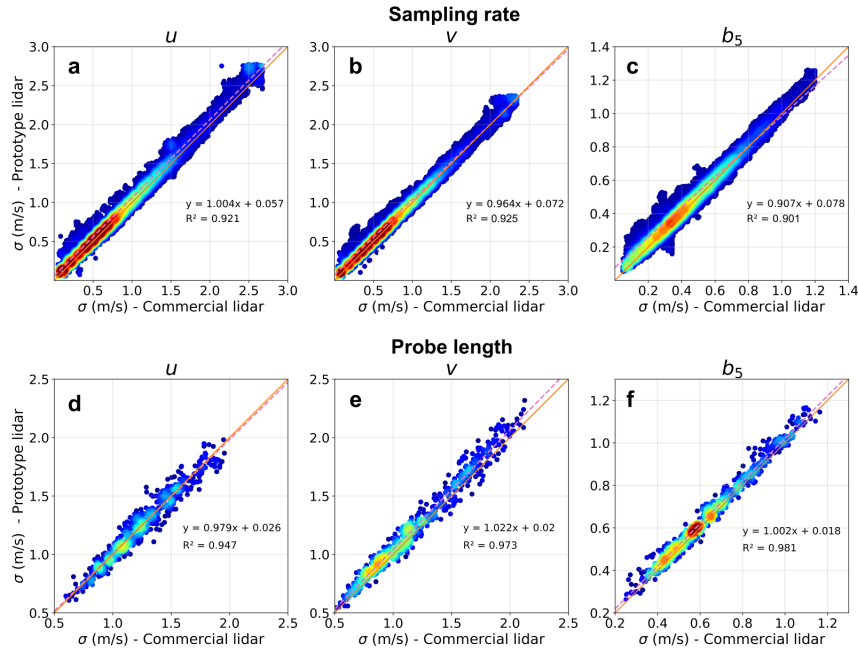
**Figure 5.** Standard deviation, $\sigma$, of the along ($u$), cross ($v$), and vertical ($b_5$) velocity components computed from prototype lidar measurements with increased sampling rate (panels a, b, c) and reduced probe length (panels d, e, f) compared to standard deviations derived from commercial lidars measurements.
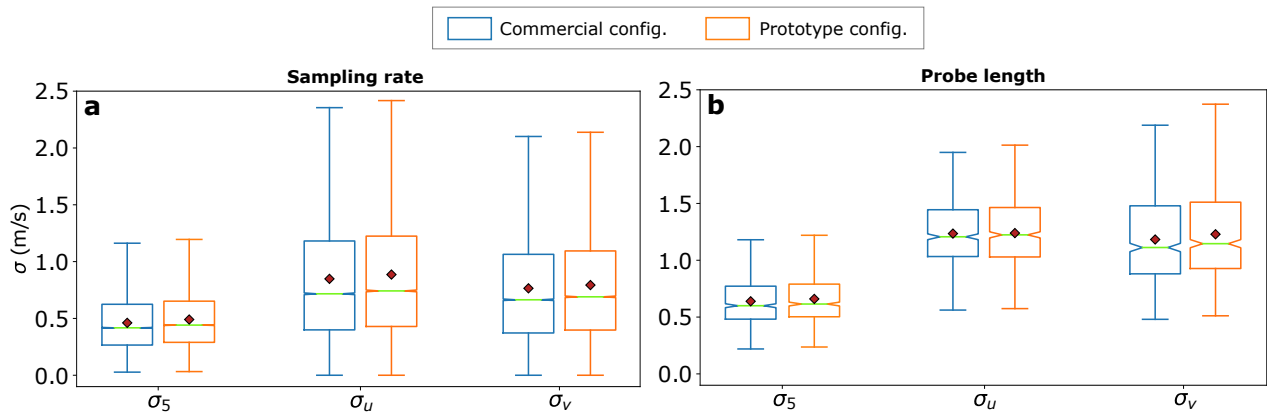
**Figure 6.** Boxplots of the standard deviation of the vertical ($\sigma_5$), along-wind ($\sigma_u$), and cross-wind ($\sigma_v$) velocities for the commercial (blue) and prototype (orange) configurations. Panels (a) and (b) correspond to the studies on increased sampling rate and reduced probe length, respectively. The medians are indicated by green lines, and the means are represented by red diamonds.

three weighting scheme applied to a measured spectrum. This iterative process was conducted across all lidar configurations, yielding consistent results described hereafter.

285   The fitted spectra closely matched in the low-frequency domain, approximately up to $f = 0.1$ Hz, but strong divergences were observed thereafter. The low frequencies weighted scheme produced a curve substantially below the measured spectra at higher frequencies, whereas the unweighted scheme yielded a curve slightly above the measured spectra in this frequency range. In contrast, the high frequencies weighted scheme provided a fit that closely matched the measured spectra across all frequencies. The optimal weighting scheme, identified as the high-frequency weighted scheme, exhibited the lowest error.

290   For instance, when applied to the prototype lidar with an enhanced sampling rate, the mean variance was 0.232 m$^2$/s$^2$ for all integrated fitted spectra using the high-frequency weighted scheme, compared to 0.226 m$^2$/s$^2$ for all integrated measured spectra. This results in an absolute error of 2.6%. Conversely, not employing any weighting during the fitting process resulted in an absolute error between the mean variance nearly three higher, at 8.5%. Assigning weights to the low frequencies resulted
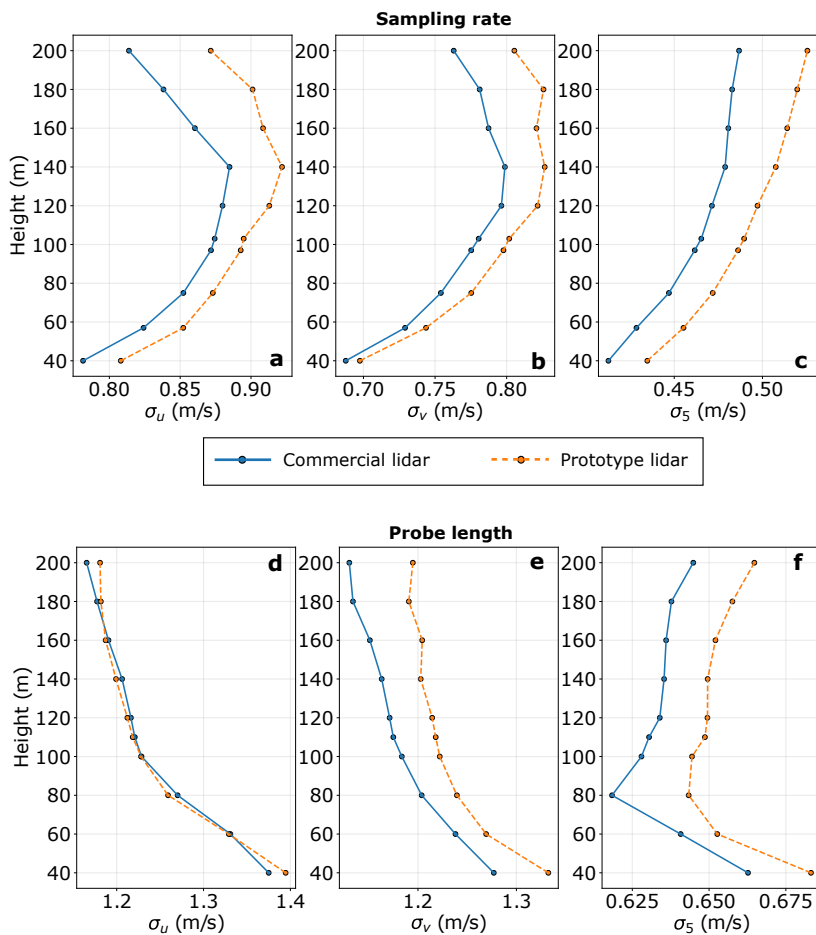
**Figure 7.** Standard deviation, $\sigma$, of the along ($u$), cross ($v$), and vertical ($b_5$) wind velocity components computed from prototype lidar measurements with increased sampling rate (panels a, b, c) and reduced probe length (panels d, e, f) compared to standard deviations derived from commercial lidars measurements.
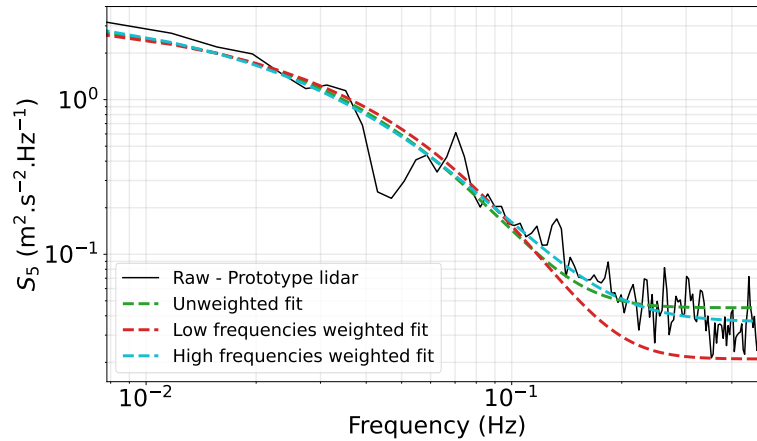
**Figure 8.** Individual LOS velocity spectrum (solid black) of the prototype lidar involving an increased sampling rate fitted with Eq. 6 with three weighted schemes: unweighted fit (dashed green), low frequencies weighted fit (dashed red), and high frequencies weighted fit (dashed blue).
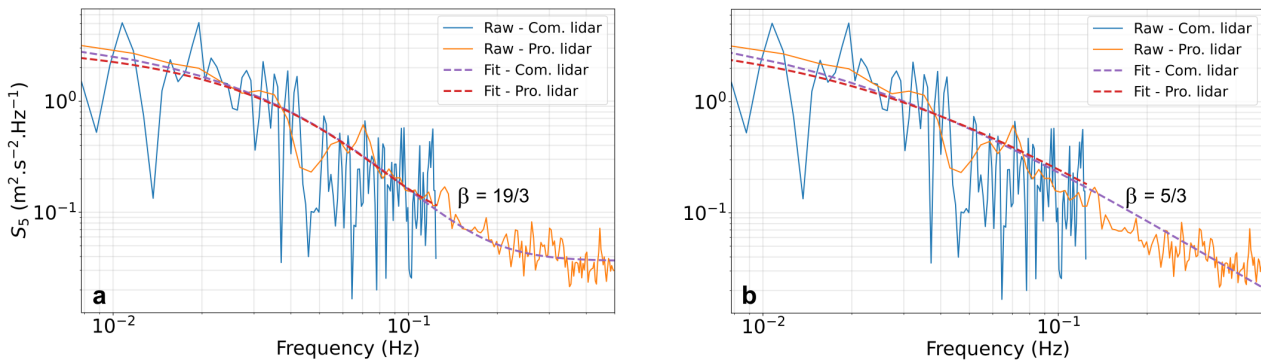
**Figure 9.** Individual LOS velocity spectrum measured by the commercial lidar (blue curve) and prototype lidar (orange curve) with increased sampling rate. The data is fitted using Eq. 6 with $\beta = 19/3$ (a) and $\beta = 5/3$ (b). The fit with $\beta = 19/3$ shows the smallest error.

in a mean absolute error exceeding six times that of the high-frequency weighted scheme, at 16.9%. Spectra derived from the

295    commercial configurations and the prototype configuration with a reduced probe length generated absolute errors that were found to be 15-20% higher than the error associated with the configuration using an increased sampling rate, regardless of the weighting scheme used.

     Theoretically, for fully developed turbulence, $\beta$ in Eq. 6 should be equal to 5/3. After fitting the spectra using the optimal weighting scheme, we sought instances where this exponent fell within the range of $5/3 \pm 0.1$. However, for any lidar configu-

300    ration, we could not achieve this condition. Instead, the median value of $\beta$ for the experiment with increased sampling rate and reduced probe length was approximately 19/3 and 18/3 respectively, which is nearly four times the theoretical value. Examples of fittings the same spectra with $\beta = 19/3$ and $\beta = 5/3$ are shown in Fig. 9.

A general observation, particularly evident in this specific example, is that the fitting of spectra derived from the commercial configuration measurements did not capture the flattened portion of the spectra characteristic of noise. Similar observations were made for fittings applied to spectra from the prototype configuration with a reduced probe length (not shown). However, for the prototype lidar with an increased sampling rate (Fig. 9a), the flattened portion was clearly reproduced by the fitting. Nonetheless, a general remark is that imposing $\beta = 5/3$ (Fig. 9b) for the fitting does not generally capture the noise portion regardless of the lidar configuration.

For measurements performed by the prototype lidar with an enhanced sampling rate, imposing $\beta = 5/3$ during fitting with the optimal scheme resulted in a mean variance of 0.235 $\mathrm{m^2/s^2}$, which is 3.9% higher than the mean variance obtained from integrating the measured spectra. This compares to a 2.6% error when $\beta$ was not imposed. A similar increase in error when imposing $\beta = 5/3$, compared to not imposing it, was also observed in measurements from other lidar configurations.

### 3.4 Noise

The impact on noise level from modifying the WindCube lidar profiler technology, in terms of sampling rate and probe length, has been evaluated by computing the interquartile ranges and mean. Fig. 10a shows that increasing the sampling rate significantly reduces both the interquartile ranges and the mean noise level compared to the commercial configuration. The prototype configuration achieves a median noise level that is 2.3 times lower than the commercial version, while the mean noise level is 4 times lower due to the high noise values within the upper 75% interquartile range. Conversely, reducing the probe length increases the mean and interquartiles of noise level by a factor of 1.2.

### 3.5 Integral length scale

A similar analysis was performed on the vertical integral length scale. Fig. 10b shows that reducing the probe length has minimal impact on the computation of the integral length scale, with mean and median values differing by less than 1% compared to the commercial configuration. However, the prototype configuration slightly reduces the upper 75% interquartile range and above. Increasing the sampling rate, however, does affect the integral length scale computation. The prototype lidar shows mean and median values that are 7% and 5% lower, respectively, than those given by the commercial configuration. Overall, all interquartile ranges were found to be lower with the prototype configuration.

### 3.6 Dissipation rate

Finally, the impact of modifying the WindCube lidar profiler technology on dissipation rate has been assessed. The dissipation rate was derived from Eq. 9 using spectra fitted with $\beta = 5/3$ (Eq. 6). However, this equation is only valid when turbulence is fully developed, i.e., when $\beta$ is higher than 1 (e.g., Neuhaus et al., 2023). Example of individual spectra derived from the prototype configuration enhancing an increased sampling rate can be found in Fig. 11 for different values of $\beta$ and thus different turbulent regimes. Spectra with a $\beta$ value lower than 1 were excluded from the analysis, resulting in the rejection of 3.4% and

3.1% of the spectra for the experiments with increased sampling rate and reduced probe length, respectively. The rejected spectra were associated with mean wind speed not exceeded 5.1 m/s.

335     The dissipation rate was computed by considering the power spectral density of noise, $N_5$, resulting from fitting spectra with $\beta$ as a free parameter, as fixing $\beta = 5/3$ often failed to properly identify the flat portion characteristic of noise in the spectra. Neglecting the noise led to dissipation rate values that were, on average, 26% higher. Fig. 10c illustrates that increasing the
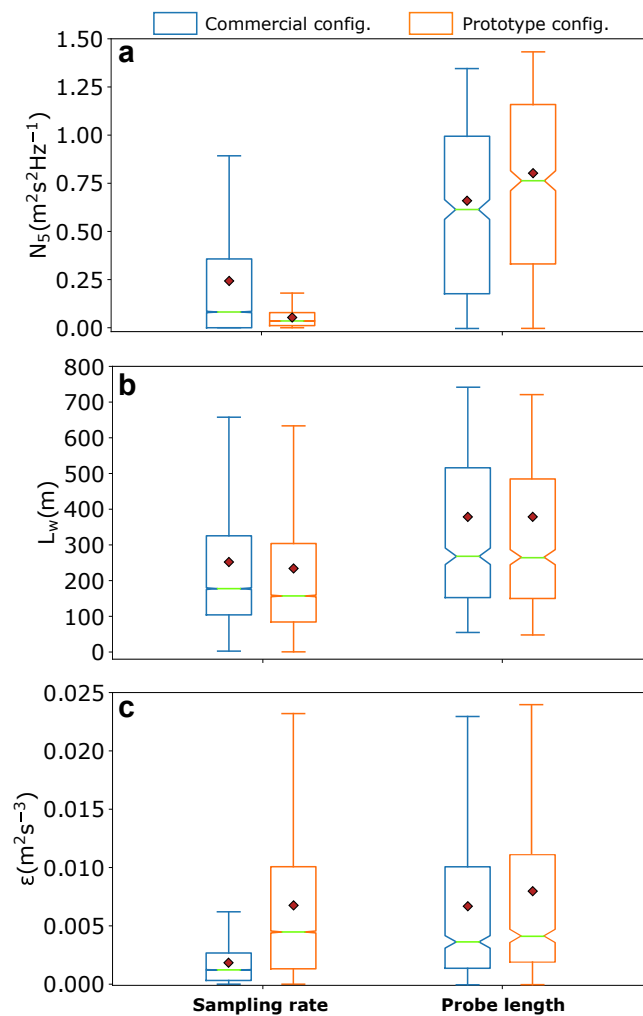
**Figure 10.** Boxplots of the standard deviation of the spectral power density of noise level, $N_5$ (a), vertical integral length scale, $L_w$ (b), and dissipation rate, $\varepsilon$ (c), for the commercial (blue) and prototype (orange) configurations. The left-hand side of each figure shows results for increased sampling rate, and the right-hand side shows results for reduced probe length.
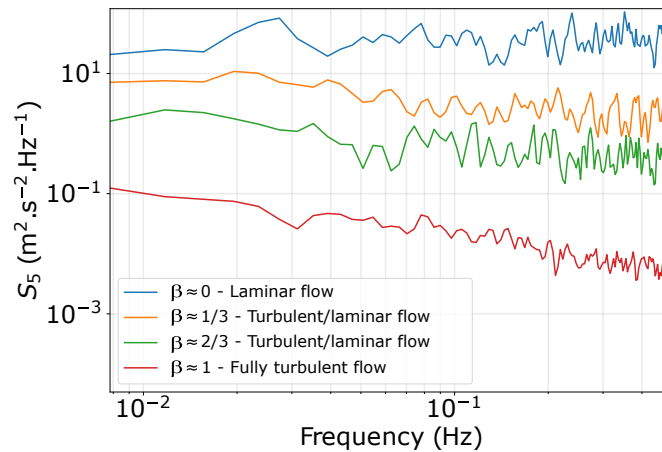
**Figure 11.** Individual LOS velocity spectra measured by beam 5 of the prototype lidar with an increased sampling rate for different turbulent regimes associated with a $\beta$ value (Eq. 6).

sampling rate resulted in a mean dissipation rate increase by a factor of 3.7 and a median increase by a factor of 4, while reducing the probe length led to a mean dissipation rate increase by a factor of 1.2 and a median increase by a factor of 1.5.

## 4 Discussion

### 4.1 Impact of increased sampling rate

The increased sampling rate in the modified lidar resulted in a systematic and slight reduction in data availability for the wind vector and a slight underestimation of mean wind speed. The reduction in data availability cannot be conclusively attributed to the increased sampling rate and, i.e., reduced accumulation time at each measurement position, as similar magnitudes of reduction could be observed when comparing two commercial configurations. Moreover, although a very slight bias in mean wind speed was found to be relatively constant across different altitudes, it is a positive outcome that the increased sampling rate does not significantly impact the measurement of mean wind speed.

In terms of turbulence measurement, the increased sampling rate configuration improved the overall accuracy of turbulence metrics. The prototype configuration showed higher standard deviations for along-wind, cross-wind, and vertical wind velocities compared to the commercial configuration. This suggests a greater sensitivity to smaller-scale fluctuations, potentially providing a more detailed representation of turbulence.

Noise levels were significantly reduced with the increased sampling rate. This reduction in noise can be attributed to the redistribution of noise along an extended frequency range, which allows for clearer differentiation between actual wind fluctuations and measurement noise. A reduction in noise level can improve the reliability of detecting true turbulent fluctuations,

355 thus enhancing the precision of turbulence measurements. The decrease in noise is a beneficial outcome, as it enhances the quality of the data collected, making it easier to distinguish between genuine turbulence and artifacts caused by noise.

The increased sampling rate also affected the integral length scale computation. The prototype lidar with an increased sampling rate showed mean and median values for the integral length scale that were lower than those given by the commercial configuration. The frequency associated with the integral length scale is linked to the peak of the energy spectrum or the
360 frequency at which a significant portion of the energy is contained. A too-low sampling rate might fail to identify this frequency, thereby missing the associated eddies. Consequently, for the commercial configuration, the integral length scale is likely sometimes overestimated, as the real energy peak might not be captured, resulting in integral length scale values that do not accurately represent the true turbulence scale. Increasing the sampling rate with the prototype configuration will reduce the number of cases where this peak is not identified. However, it does not guarantee that the new sampling rate will always
365 capture the part of the spectrum with the most energy. Nonetheless, it is likely to provide values closer to reality compared to the commercial lidar configuration.

The increased sampling rate also demonstrated an improvement in fitting velocity spectra with a parametric expression. The error, computed in terms of variance derived from the measured spectra and associated fitted spectra, was found to be up to 20% lower than that of the commercial configurations and the configuration with a reduced probe length. This improvement
370 directly impacts the calculation of the dissipation rate deduced from the fitted spectra. The dissipation rate computed from the configuration with the increased sampling rate was found to be up to four times higher than that derived from the commercial configuration. This is because the prototype configuration captures an extended inertial subrange, resulting in more accurate values of the dissipation rate.

## 4.2 Impact of reduced probe length

375 The reduced probe length did not impact the data availability of the wind vector but led to an overestimation of mean wind speed, with significant bias particularly pronounced at lower altitudes. This overestimation, which peaks at over 4% at 40 m above the ground, indicates that while a shorter probe length may improve the resolution of smaller-scale eddies, it introduces substantial inaccuracies in mean wind speed measurements. This bias does not correlate with wind speed or CNR, suggesting that other factors related to probe length and measurement volume may be influencing these discrepancies.

380 In terms of turbulence measurement, the reduced probe length configuration also exhibited higher standard deviations, though to a lesser extent than the increased sampling rate configuration. This points to a potential improved sensitivity to smaller eddies, but with the trade-off of introducing more noise into the measurements. The increased noise levels indicate that while the shorter probe length might enhance the capture of smaller-scale fluctuations, it does so at the cost of increased measurement noise, potentially complicating the interpretation of turbulence data.

385 However, the reduced probe length had minimal impact on the integral length scale, with mean and median values differing by less than 1% from the commercial configuration. This lack of impact is expected, as the probe length of the commercial lidar is 23 m and that of the prototype lidar is 15 m, both of which are much smaller than the integral length scale of the turbulence being measured. Consequently, the modification of the probe length does not affect the measurement of large eddies.

Reducing the probe length was expected to enhance the representation of the inertial subrange, as the probe length of the
390  commercial and prototype configurations directly influences turbulence length scales within this range. However, it was found
that, on average, the slope of the spectra, which is supposed to manifest the energy cascade of the inertial subrange, remained
similar for both configurations.

## 5  Conclusion

This study investigates potential modifications to the WindCube v2.1 lidar profiler - specifically, increased sampling rate and
395  reduced probe length - to enhance turbulence measurement. The findings offer a detailed analysis of how these changes impact
various wind measurement aspects, including mean wind speed, standard deviation, velocity spectra, noise level, integral length
scale, and dissipation rate.

The prototype configuration, with an increased sampling rate, samples four times faster than the commercial configuration.
This enhancement improves turbulence measurement without affecting mean wind speed measurement. However, a slight
400  reduction in data availability was observed compared to the commercial configuration. Despite this, the reduction is minimal
enough to allow for further exploration of increased sampling rates to enhance turbulence measurement. Nonetheless, the
potential for further increasing the sampling rate is very limited. The prototype configuration already involves a 70% reduction
in accumulation time at each LOS measurement position, and further reductions could significantly impact the accuracy of
mean wind statistics, which is the primary objective of wind lidar profiler.

405  The reduced probe length, which entails a 50% reduction in pulse duration compared to the commercial configuration, did
not show similar improvements in turbulence measurement. While improvements in turbulent fluctuations were comparable
to those achieved with the increased sampling rate, they came at the expense of increased noise levels. This makes it unclear
whether the higher standard deviations are due to the energy of smaller eddies or noise. Moreover, the reduced probe length
configuration exhibited a high bias in mean wind speed measurement compared to the commercial configuration, which is a
410  significant issue for industrial-scale deployment. However, the data length for the reduced probe length experiment might be
too short to draw definitive conclusions, necessitating a longer experiment for conclusive results.

Ideally, the optimal configuration for the WindCube lidar would involve both an increased sampling rate and a reduced
probe length, translating to reduced accumulation time with shorter pulse duration. Unfortunately, such a configuration would
likely result in poor data availability and questionable accuracy in mean wind statistics. Therefore, only one modification can
415  be effectively implemented in the WindCube lidar, with the increased sampling rate being the most promising for improving
turbulence measurement without affecting mean wind speed measurement.

**Author contributions**

MT identified the problematic, performed the analysis and drafted the paper. FD and CB contributed to the development and establishment of the two tailored versions of the WindCube v2.1 proposed in this paper and reviewed the manuscript. FG
420 reviewed the manuscript.

**Data and code availability**

The data is owned by a private consortium with proprietary rights and confidentiality obligations, precluding its sharing alongside this paper.

**Competing interest**

425 The authors declare that they have no conflict of interest.

**Financial support**

This work was made possible through the support of France Energies Marines and the French government, managed by the Agence Nationale de la Recherche under the Investissements d'Avenir program, with the reference ANR-10-IEED-0006-34. This work was carried out in the framework of the POWSEIDOM project.

## References

Bodini, N., Lundquist, J. K., and Newsom, R. K.: Estimation of turbulence dissipation rate and its variability from sonic anemometer and wind Doppler lidar during the XPIA field campaign, Atmospheric Measurement Techniques, 11, 4291–4308, 2018.

Bodini, N., Lundquist, J. K., Krishnamurthy, R., Pekour, M., Berg, L. K., and Choukulkar, A.: Spatial and temporal variability of turbulence dissipation rate in complex terrain, Atmospheric Chemistry and Physics, 19, 4367–4382, 2019.

Branlard, E., Pedersen, A. T., Mann, J., Angelou, N., Fischer, A., Mikkelsen, T., Harris, M., Slinger, C., and Montes, B. F.: Retrieving wind statistics from average spectrum of continuous-wave lidar, Atmospheric Measurement Techniques, 6, 1673–1683, 2013.

Browning, K. A. and Wexler, R.: The determination of kinematic properties of a wind field using Doppler radar, Journal of Applied meteorology and climatology, 7, 105–113, 1968.

Durgesh, V., Thomson, J., Richmond, M. C., and Polagye, B. L.: Noise correction of turbulent spectra obtained from acoustic doppler velocimeters, Flow Measurement and Instrumentation, 37, 29–41, 2014.

Eberhard, W. L., Cupp, R. E., and Healy, K. R.: Doppler lidar measurement of profiles of turbulence and momentum flux, Journal of Atmospheric and Oceanic Technology, 6, 809–819, 1989.

Frehlich, R.: Estimation of velocity error for Doppler lidar measurements, Journal of Atmospheric and Oceanic Technology, 18, 1628–1639, 2001.

Gal-Chen, T., Xu, M., and Eberhard, W. L.: Estimations of atmospheric boundary layer fluxes and other turbulence parameters from Doppler lidar data, Journal of Geophysical Research: Atmospheres, 97, 18 409–18 423, 1992.

Guerra, M. and Thomson, J.: Turbulence Measurements from Five-Beam Acoustic Doppler Current Profilers, Journal of Atmospheric and Oceanic Technology, 34, 1267–1284, 2017.

International Electronical Commission: IEC 61400-12-1. Wind energy generation systems – Part 12-1: Power performance measurements of electricity producing wind turbines. Edition 2.0, 2017.

Kelberlau, F. and Mann, J.: Cross-contamination effect on turbulence spectra from Doppler beam swinging wind lidar, Wind Energy Science, 5, 519–541, 2020.

Kropfli, R. A.: Single Doppler radar measurements of turbulence profiles in the convective boundary layer, Journal of Atmospheric and Oceanic Technology, 3, 305–314, 1986.

Lhermitte, R. M.: Note on wind variability with Doppler radar, Journal of Atmospheric Sciences, 19, 343–346, 1962.

Lhermitte, R. M.: Note on the observation of small-scale atmospheric turbulence by Doppler radar techniques, Radio Science, 4, 1241–1246, 1969.

Lothon, M., Lenschow, D. H., and Mayor, S. D.: Doppler lidar measurements of vertical velocity spectra in the convective planetary boundary layer, Boundary-layer meteorology, 132, 205–226, 2009.

Mann, J., Cariou, J.-P., Courtney, M. S., Parmentier, R., Mikkelsen, T., Wagner, R., Lindelow, P., Sjoholm, M., and Enevoldsen, K.: Comparison of 3D turbulence measurements using three staring wind lidars and a sonic anemometer, Meteorologische Zeitschrift, 18, 135, 2009.

Mann, J., Peña, A., Bingöl, F., Wagner, R., and Courtney, M. S.: Lidar scanning of momentum flux in and above the atmospheric surface layer, Journal of Atmospheric and Oceanic Technology, 27, 959–976, 2010.

McMillan, J. M. and Hay, A. E.: Spectral and structure function estimates of turbulence dissipation rates in a high-flow tidal channel using broadband ADCPs, Journal of Atmospheric and Oceanic Technology, 34, 5–20, 2017.

Neuhaus, L., Wächter, M., and Peinke, J.: The fractal turbulent/non-turbulent interface in the atmosphere, Wind Energy Science Discussions, 2023, 1–19, 2023.

Olesen, H. R., Larsen, S. E., and Højstrup, J.: Modelling velocity spectra in the lower part of the planetary boundary layer, Boundary-Layer
470     Meteorology, 29, 285–312, 1984.

O'Connor, E. J., Illingworth, A. J., Brooks, I. M., Westbrook, C. D., Hogan, R. J., Davies, F., and Brooks, B. J.: A method for estimating the turbulent kinetic energy dissipation rate from a vertically pointing Doppler lidar, and independent evaluation from balloon-borne in situ measurements, Journal of atmospheric and oceanic technology, 27, 1652–1664, 2010.

Peña, A., Hasager, C. B., Gryning, S., Courtney, M., Antoniou, I., and Mikkelsen, T.: Offshore wind profiling using light detection and
475     ranging measurements, Wind Energy, 12, 105–124, 2009.

Pope, S. B.: Turbulent flows, Cambridge University Press, 2000.

Sathe, A. and Mann, J.: Measurement of turbulence spectra using scanning pulsed wind lidars, Journal of Geophysical Research: Atmospheres, 117, 2012.

Sathe, A., Mann, J., Gottschall, J., and Courtney, M. S.: Can wind lidars measure turbulence?, Journal of Atmospheric and Oceanic Technol-
480     ogy, 28, 853–868, 2011.

Sathe, A., Mann, J., Vasiljevic, N., and Lea, G.: A six-beam method to measure turbulence statistics using ground-based wind lidars, Atmospheric Measurement Techniques, 8, 729–740, 2015.

Sjöholm, M., Mikkelsen, T., Mann, J., Enevoldsen, K., and Courtney, M.: Spatial averaging-effects on turbulence measured by a continuous-wave coherent lidar, Meteorologische Zeitschrift (Berlin), 18, 2009.

485  Smalikho, I., Köpp, F., and Rahm, S.: Measurement of atmospheric turbulence by 2-$\mu$ m Doppler lidar, Journal of Atmospheric and Oceanic Technology, 22, 1733–1747, 2005.

Sreenivasan, K. R.: On the universality of the Kolmogorov constant, Physics of Fluids, 7, 2778–2784, 1995.

Strauch, R. G., Merritt, D. A., Moran, K. P., Earnshaw, K. B., and De Kamp, D. V.: The Colorado wind-profiling network, Journal of Atmospheric and Oceanic Technology, 1, 37–49, 1984.

490  Stull, R. B.: Meteorology for scientists and engineers: a technical companion book with Ahrens' Meteorology Today, publisher: Brooks/Cole Boston, 2000.

Teunissen, H. W.: Structure of mean winds and turbulence in the planetary boundary layer over rural terrain, Boundary-Layer Meteorology, 19, 187–221, 1980.

Thiébaut, M., Filipot, J.-F., Maisondieu, C., Damblans, G., Duarte, R., Droniou, E., Chaplain, N., and Guillou, S.: A comprehensive assess-
495     ment of turbulence at a tidal-stream energy site influenced by wind-generated ocean waves, Energy, 191, 116 550, 2020a.

Thiébaut, M., Filipot, J.-F., Maisondieu, C., Damblans, G., Duarte, R., Droniou, E., and Guillou, S.: Assessing the turbulent kinetic energy budget in an energetic tidal flow from measurements of coupled ADCPs, Philosophical Transactions of the Royal Society A, 378, 20190 496, 2020b.

Thiébaut, M., Quillien, N., Maison, A., Gaborieau, H., Ruiz, N., MacKenzie, S., Connor, G., and Filipot, J.-F.: Investigating the flow dynamics
500     and turbulence at a tidal-stream energy site in a highly energetic estuary, Renewable Energy, 195, 252–262, 2022.

Thomson, J., Polagye, B., Durgesh, V., and Richmond, M. C.: Measurements of turbulence at two tidal energy sites in Puget Sound, WA, Oceanic Engineering, IEEE Journal of Oceanic Engineering, 37, 363–374, 2012.

Tieleman, H. W.: Universality of velocity spectra, Journal of Wind Engineering and Industrial Aerodynamics, 56, 55–69, 1995.

Tonttila, J., O'Connor, E. J., Hellsten, A., Hirsikko, A., O'Dowd, C., Järvinen, H., and Räisänen, P.: Turbulent structure and scaling of the inertial subrange in a stratocumulus-topped boundary layer observed by a Doppler lidar, Atmospheric chemistry and physics, 15, 5873–5885, 2015.

Tritton, D. J.: Physical fluid dynamics, Springer Science & Business Media, 2012.

Welch, P.: The use of fast Fourier transform for the estimation of power spectra: A method based on time averaging over short, modified periodograms, IEEE Transactions on audio and electroacoustics, 15, 70–73, 1967.

Wildmann, N., Bodini, N., Lundquist, J. K., Bariteau, L., and Wagner, J.: Estimation of turbulence dissipation rate from Doppler wind lidars and in situ instrumentation for the Perdigão 2017 campaign, Atmospheric Measurement Techniques, 12, 6401–6423, 2019.

Wilson, D. A.: Doppler radar studies of boundary layer wind profile and turbulence in snow conditions, 1970.